

Research Article

Effect of New Analogs of Hexyloxy Phenyl Imidazoline on Quorum Sensing in *Chromobacterium violaceum* and *In Silico* Analysis of Ligand-Receptor Interactions

José Luis Herrera-Arizmendi,¹ Everardo Curiel-Quesada,² José Correa-Basurto ,³ Martiniano Bello,³ and Alicia Reyes-Arellano ¹

¹Departamento de Química Orgánica, Escuela Nacional de Ciencias Biológicas, Instituto Politécnico Nacional, Carpio y Plan de Ayala S/N, Colonia Santo Tomás, 11340 Ciudad de México, Mexico

²Departamento de Bioquímica, Escuela Nacional de Ciencias Biológicas, Instituto Politécnico Nacional, Carpio y Plan de Ayala S/N, Colonia Santo Tomás, 11340 Ciudad de México, Mexico

³Escuela Superior de Medicina, Laboratorio de Diseño y Desarrollo de Nuevos Fármacos e Innovación Biotecnológica, Instituto Politécnico Nacional, 11340 Ciudad de México, Mexico

Correspondence should be addressed to Alicia Reyes-Arellano; areyesarellano@yahoo.com.mx

Received 16 October 2019; Accepted 30 December 2019; Published 25 February 2020

Academic Editor: Oliver Sutcliffe

Copyright © 2020 José Luis Herrera-Arizmendi et al. This is an open access article distributed under the Creative Commons Attribution License, which permits unrestricted use, distribution, and reproduction in any medium, provided the original work is properly cited.

The increasing common occurrence of antibiotic-resistant bacteria has become an urgent public health issue. There are currently some infections without any effective treatment, which require new therapeutic strategies. An attractive alternative is the design of compounds capable of disrupting bacterial communication known as *quorum sensing* (QS). In Gram-negative bacteria, such communication is regulated by acyl-homoserine lactones (AHLs). Triggering of QS after bacteria have reached a high cell density allows them to proliferate before expressing virulence factors. Our group previously reported that hexyloxy phenylimidazoline (**9**) demonstrated 71% inhibitory activity of QS at 100 μM ($\text{IC}_{50} = 90.9 \mu\text{M}$) in *Chromobacterium violaceum*, a Gram-negative bacterium. The aim of the present study was to take **9** as a lead compound to design and synthesize three 2-imidazolines (**13–15**) and three 2-oxazolines (**16–18**), to be evaluated as *quorum-sensing* inhibitors on *C. violaceum* CV026. We were looking for compounds with a higher affinity towards the Cvi receptor of this bacterium and the ability to inhibit QS. The binding mode of the test compounds on the Cvi receptor was explored with docking studies and molecular dynamics. It was found that 8-pentyloxyphenyl-2-imidazoline (**13**) reduced the production of violacein ($\text{IC}_{50} = 56.38 \mu\text{M}$) without affecting bacterial growth, suggesting inhibition of *quorum sensing*. Indeed, compound **13** is apparently one of the best QS inhibitors known to date. Molecular docking revealed the affinity of compound **13** for the orthosteric site of *N*-hexanoyl homoserine lactone (C_6 -AHL) on the CviR protein. Ten amino acid residues in the active binding site of C_6 -AHL in the Cvi receptor interacted with **13**, and 7 of these are the same as those interacting with AHL. Contrarily, 8-octyloxyphenyl-2-imidazoline (**14**), 8-decyloxyphenyl-2-imidazoline (**15**), and 9-decyloxyphenyl-2-oxazoline (**18**) bound only to an allosteric site and thus did not compete with C_6 -AHL for the orthosteric site.

1. Introduction

The *quorum sensing* (QS) is a mechanism of bacterial communication involved in regulating the expression of genes linked to the production of virulence factors, among other functions. Such virulence factors include lytic enzymes, proteases, siderophores, and adhesins [1–3]. This

mechanism is based on the detection of small signaling molecules called autoinducers or semiochemicals, which are synthesized and released when bacteria reach a certain population density [4].

Interrupting QS is an attractive strategy in the fight against bacteria, especially against pharmaco-resistant bacteria because the QS break does not directly affect the

survival of these microorganisms [5]. Given the increasingly common antibiotic resistance displayed by bacteria, particularly in the case of hospital infections, there is an intense search for novel antibacterial agents. Hence, the development of *quorum-sensing* inhibitors (QSIs), also known as *antiquorum-sensing* (antiQS) molecules, could possibly be an important element in the development of new antimicrobial agents.

Compounds that function as QSIs can be obtained from plants (2 and 3) [6], bacteria [7], marine algae (4 and 5) [8], fungi (6) [9], and synthetic procedures (7, 8, and 9) [10–12]. In Gram-negative bacteria, the QS system is regulated by acyl-homoserine lactones (AHLs). Bacterial enzymes of some Gram-positive bacteria like the *Bacillus* species interfere with QS via an AHL-lactonase [13], Figure 1. Various analogs and bioisosteres of AHLs have been synthesized as inhibitors of Gram-negative bacteria [12], and some of them designed to interfere with QS in *Chromobacterium violaceum* [14].

Chromobacterium violaceum is a Gram-negative bacterium whose autoinducer is hexanoyl homoserine lactone (C_6 -AHL, 1). *C. violaceum* was herein used as a biosensor [15].

Our group previously observed [12] the potential of imidazoline 9 as a lead compound, evidenced by its 71% inhibitory activity of QS in *C. violaceum* at 100 μ M ($IC_{50} = 90.9 \mu$ M). In the present study, we sought analogs of compound 9 with improved inhibitory activity. In addition to carrying out inhibition assays of the test compounds on *C. violaceum*, docking and molecular dynamics studies were performed with the same compounds to gain insights into the interactions responsible for the desired activity.

2. Results and Discussion

2.1. Chemistry. Six azolines were synthesized, including three 8-alkyloxyphenyl-2-imidazolines and three 9-alkyloxyphenyl-2-oxazolines, with moderate and good yields, respectively (Table 1).

Compound 13 has been synthesized and mediated by pentyloxybenzene, 4-aminobutanoic acid, phosphoric acid, and P_2O_5 , with yield 48% [16]. It was here synthesized with a better yield as shown in Table 1. Compound 14 has already been synthesized by 4-octyloxybenzotrile and ethylenediamine, with yield 50% [17]. Here, it was obtained with a yield of 79%. Compound 15 was reported by Gossens et al. [18] as a precursor of an ionic liquid, but melting point, yield and, spectroscopic data are missing. They obtained compound 15 mediated by ethylenediamine and NBS. Attempts to obtain the 16, 17, and 18 compounds by conventional heat gave only traces of the compounds after a long time. Contrariwise, microwave energy gave good yields in short times. Compounds 16–18 are new. Compounds 13–18 have never been employed as a QSI.

All compounds were characterized by spectroscopic methods (IR, NMR, and HRMS), identifying 8-pentyloxyphenyl-2-imidazoline (13), 8-octyloxyphenyl-2-imidazoline (14), 8-decyloxyphenyl-2-imidazoline (15), 9-pentyloxyphenyl-2-oxazoline (16), 9-octyloxyphenyl-2-oxazoline (17), and 9-decyloxyphenyl-2-oxazoline (18).

2.2. Biological Activity

2.2.1. Evaluation of Azolines 13–18 as Quorum-Sensing Inhibitors in *Chromobacterium violaceum* CV026. After synthesizing the azolines 13–18, all were examined as possible QSIs in *C. violaceum* CV026. Since this Gram-negative bacterial strain does not synthesize its own C_6 -AHL, the production of violacein depends on the concentration of exogenous C_6 -AHL added to the medium.

Compounds 13–18 were evaluated as QSIs at 0 (blank), 0.1, 1, 10, 100, and 1000 μ M (Figure 2). Two readings were taken on a spectrophotometer to determine optical density, one at 720 nm for the culture and the other at 577 nm for the extraction of violacein. Bacterial density is usually measured at 600 or 660 nm. Since violacein absorbs at these wavelengths, we had to use 720 nm. These readings were used to calculate the relative violacein production, dividing the absorbance value at 577 nm by that found at 720 nm. For calculating the percentage of relative violacein production after the application of each test compound, the average of the values of the blanks was taken as 100%. The resulting percentage of violacein production was plotted as a function of the concentration of the compound. Our group previously reported [12] that a concentration of 500 nM of C_6 -AHL makes it easier to detect the production of violacein and its inhibition by a compound.

In the range of 0.1 to 1 μ M, compounds 13–18 did not cause a decrease in the percentage of violacein production. However, when the bacterium was exposed to a concentration $\geq 10 \mu$ M of compounds 14, 15, 16, and 18, there was a significantly higher percentage of violacein production compared to the control (Figure 2). In contrast, compounds 13 and 17 at the same concentration did not stimulate such an increase in production. In fact, violacein production significantly declined with 13 between 100 μ M and 1000 μ M due to a toxic effect on bacteria at these concentrations.

Although three oxazolines elevated the production of violacein at 100 μ M, only two of them, oxazolines 17 and 18, did so at 1000 μ M. The latter two compounds did not have any effect on the growth of *C. violaceum* CV026. On the contrary, imidazoline 15 at a concentration of 100 and 1000 μ M did not trigger violacein production, but instead had an inhibitory effect on the growth of bacteria, which was verified by the viable count. The same effect was observed with 1000 μ M of oxazoline 16. Since the 10 and 100 μ M concentrations of imidazoline 13 prompted an abrupt decrease in violacein production, an experiment was conducted with concentrations of 0–100 μ M (Figure 3).

Imidazoline 13 showed a dose-dependent behavior (Figure 3). A viable count was made between 30 and 100 μ M. Colony growth was observed between 30 and 90 μ M. At 100 μ M, colony growth was not observed; therefore, the reduction in violacein production can be attributed to QSI activity between 30 and 90 μ M, Figure 3. According to the experimental data, the IC_{50} was calculated to be 56.38 μ M. This value can be compared to those reported by Bucio-Cano et al. for 9, 19–23 [12, 14], 24, and the other synthesized inhibitors [19] (Figure 4).

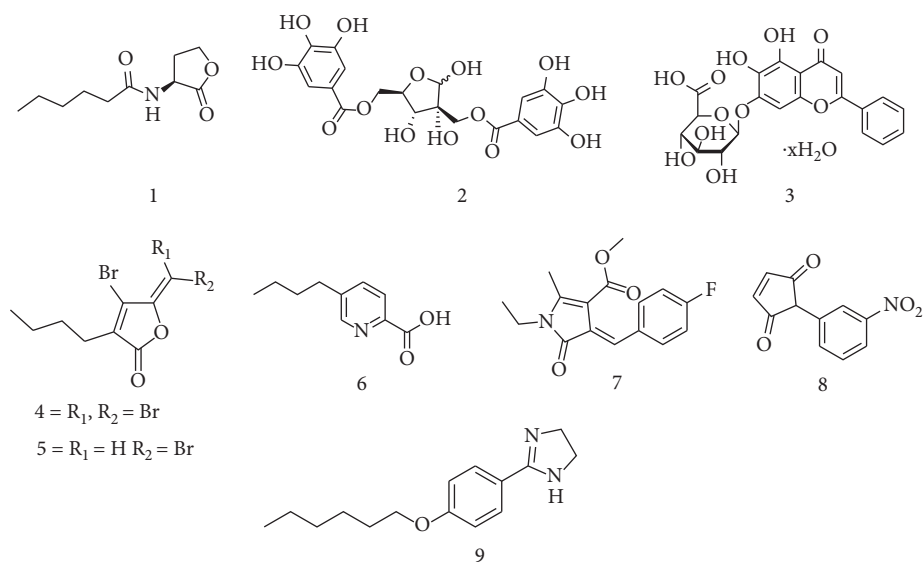
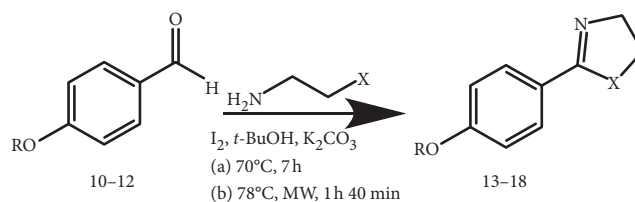
FIGURE 1: C₆-AHL (1) and some known quorum-sensing inhibitors (2–9).

TABLE 1: Synthesis of azolines.



R	X	Reaction conditions	Compound number	Isolated yield (%)
<i>n</i> -C ₅ H ₁₁	NH	(a)	13	80
<i>n</i> -C ₈ H ₁₇	NH	(a)	14	79
<i>n</i> -C ₁₀ H ₂₁	NH	(a)	15	69
<i>n</i> -C ₅ H ₁₁	O	(b)	16	89
<i>n</i> -C ₈ H ₁₇	O	(b)	17	80
<i>n</i> -C ₁₀ H ₂₁	O	(b)	18	68

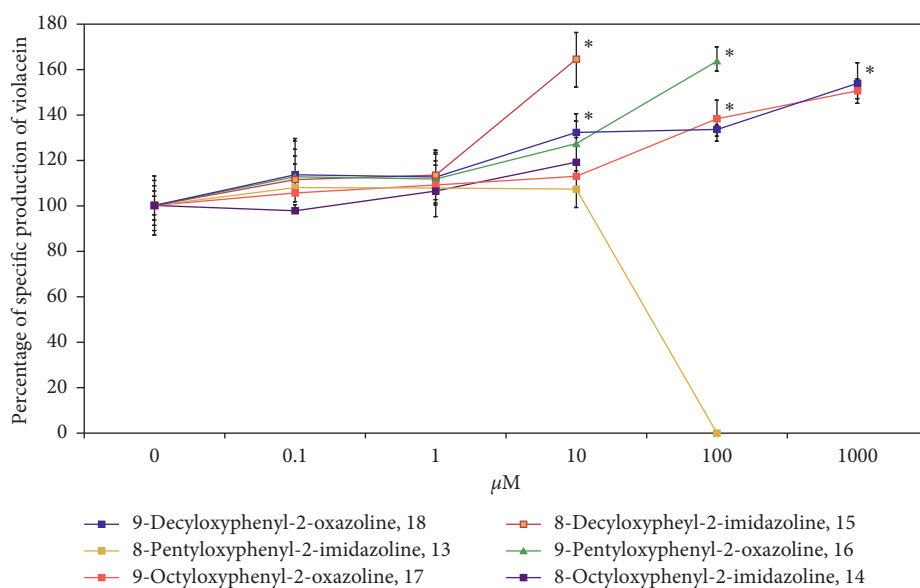


FIGURE 2: Production of violacein upon exposure to azolines 13–18. Asterisks denote statistically significant differences.

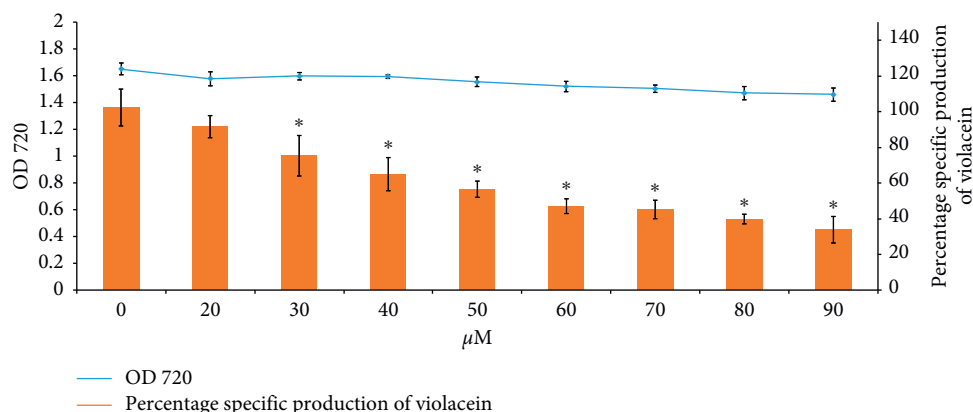


FIGURE 3: Bacterial growth (OD720 nm) and percentage of violacein production (mean \pm SE; $n = 6$) in *Chromobacterium violaceum* CV026 when exposed to different concentrations (0–100 μM) of **13**. Asterisks indicate statistically significant activity ($p < 0.05$, calculated with ANOVA).

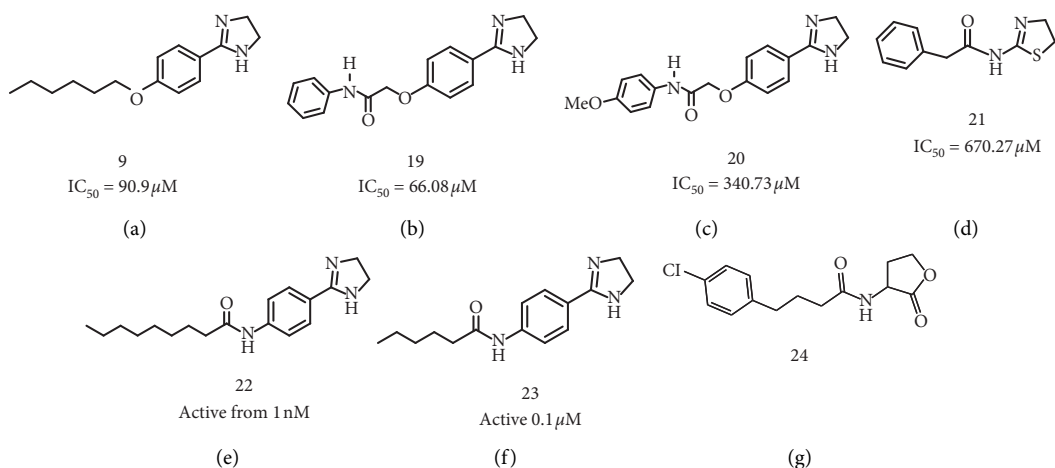


FIGURE 4: IC_{50} of some azolines [12, 14] and chlorophenoxy-*N*-butanoyl homoserine lactone **24** [19] evaluated as QSIs in *Chromobacterium violaceum* CV026. ND = not determined.

Imidazoline **13** ($\text{IC}_{50} = 56.38 \mu\text{M}$) is more active than **9** ($90.9 \mu\text{M}$) [12], **19** ($66.08 \mu\text{M}$), **20** ($340.73 \mu\text{M}$), and **21** ($670.27 \mu\text{M}$) [14] and is comparable to 2-(4'-chlorophenoxy)-*N*-butanoyl homoserine lactone **24** [19]. The latter is proposed as the most active analog of AHL known so far, giving 100% inhibition of violacein at 10^{-4} M.

Bucio et al. [12] did not give the IC_{50} value for *N*-[4-phenyl-(imidazo-2-yl)]-hexylamide, **23**, or *N*-[4-phenyl-(imidazo-2-yl)]-nonamide, **22**. However, **23** was described as QSI active from $0.1 \mu\text{M}$. Compound **22** showed an inhibitory effect on violacein production starting at a concentration of 1 nM, but the highest inhibition was 49% at $100 \mu\text{M}$. Imidazoline **13** was herein found to be active as of $30 \mu\text{M}$. Since it was essential to examine the possibility that **13** works as an antagonist of C_6 -AHL in *C. violaceum* CV026, a docking study was carried out for this ligand on the CviR protein.

2.2.2. Evaluation of Imidazolines and Oxazolines as Agonists of C_6 -AHL in *Chromobacterium violaceum* CV026. It was also crucial to determine whether the oxazolines **16–18** work as agonists of C_6 -AHL in *C. violaceum*. Therefore, *C.*

violaceum CV026 was incubated in the presence of each of the compounds at concentrations of 0.1, 1, 10, 100, and $1000 \mu\text{M}$, at 29°C and 700 rpm for 24 h, without exogenous C_6 -AHL. A positive control with C_6 -AHL and a negative control without C_6 -AHL were included. No violacein production was observed in any of the tubes containing the compounds.

Other cases of overproduction of violacein have been documented [12, 15, 20]. In 2004, Martinelli et al. [20] investigated several compounds in relation to their capacity to affect bacteria growth and/or activate QS in *C. violaceum* CV026 to improve the production of violacein. The most outstanding of their findings for the purposes of the current contribution is that some compounds are capable of stimulating violacein production, but only in the presence of C_6 -AHL. They proposed that these compounds may either bind synergistically with C_6 -AHL at the protein receptor site or interact with a second autoinductor system like the one detected in *V. harveyi*. On the contrary, Kothari and co-workers [15] suggested that enhanced violacein production is due to overexpression of the genes participating in glucose metabolism, which after some steps would affect tryptophan

biosynthesis and finally violacein biosynthesis. According to the current results, the compounds capable of elevating violacein production only did so in the presence of C₆-AHL, clearly showing that the test compounds did not perform the same function as AHL.

2.3. Docking Simulations. Ligand-protein exploration was made by means of molecular docking as to whether each compound can decrease or increase violacein production by binding to the target site on the protein. Docking was carried out with the AutoDock 4.2 Program [21]. The prior validation of docking studies involved the natural ligand C₆-AHL and the CviR protein, yielding a free energy value (ΔG) of -7.11 kcal/mol. The C₆-AHL protein made four hydrogen bond interactions with amino acid residues of the CviR active site region: (1) the carbonyl of the lactone ring with Tyr80, (2) the alpha oxygen of the lactone ring with Trp84, (3) the hydrogen of the amide with Asp97, and (4) the oxygen of the amide with Ser155. The respective distances of these four bonds were 2.56, 2.95, 2.94, and 3.28 Å, Figure 5.

The present data from the docking study of C₆-AHL on CviR coincide with the results obtained by Bucio-Cano et al. [14], who found a ΔG of -7.26 kcal/mol and the following amino acid residues in the binding region: Tyr80, Trp84, Tyr88, Asp97, Ile99, Trp111, Phe115, and Ser155, Figure 6.

Once the docking method was validated by a simulation using a natural ligand, theoretical calculations were made for the other ligands, finding the ΔG values for the interactions and identifying the amino acid residues of CviR involved in protein-ligand binding with each compound, Table 2.

The map of residues coordinating the binding of the test ligands, Table 2, suggests that there are two binding sites for the CviR protein. One is the orthosteric site of C₆-AHL, the binding location of 8-pentyloxyphenyl-2-imidazoline, 9-pentyloxyphenyl-2-oxazoline, and 9-octyloxyphenyl-2-oxazoline. The amino acid residues most frequently involved in interactions with these compounds are Tyr80, Trp84, Tyr88, Asp97, Ile99, Trp111, Phe115, Phe126, Met135, Ile153, and Ser155. The other binding site for the CviR protein is allosteric, the binding location of **16**, **17**, and **20**, most frequently involving the following residues: Ile28, Ala31, Gly32, His177, His179, Gln180, Ala181, Val183, Arg184, Leu188, and Pro190. Based on the aforementioned data, a 3D image was constructed to illustrate the overlap of the ligands in their respective binding sites, Figure 7.

The noncovalent interactions of each ligand at the orthosteric site of the CviR protein are presently described. Two hydrogen bonds are formed by the interaction of 8-pentyloxyphenyl-2-imidazoline, **13**, with the CviR protein, one between the oxygen of the ether and the Ser155 residue at a distance of 2.76 Å, and the other between the hydrogen of the imidazoline ring and Asp97 at a distance of 3.16 Å. There are also hydrophobic interactions (Van der Waals), which occur with the amino acid residues Val59, Met72, Tyr80, Trp84, Leu85, Tyr88, Ile99, Met100, Trp111, Phe115, Phe126, Met135, and Ile153, Figure 8. Additionally, π - π interactions are observed between the phenyl ring and Trp111, Figure 9.

Compound **16** forms two hydrogen bonds, one between the oxygen of the ether and Ser155 and the other between the N of the oxazoline ring and the hydrogen of Trp84. There are also hydrophobic interactions with amino acids Ile57, Tyr80, Leu85, Tyr88, Asp97, Ile99, Trp111, Phe115, Met135, and Ile153, Figure 10.

Oxazoline **17** exhibits only hydrophobic interactions with amino acids Ile57, Val59, Met72, Val75, Tyr80, Trp84, Leu85, Tyr88, Ile99, Met100, Trp111, Met135, Ile153, and Ser155, Figure 11.

Regarding the interactions between the ligands and the allosteric site, imidazoline **14** displays hydrophobic interactions with the amino acids Ile28, Ala31, Gly32, His177, Gln180, Ala181, Val183, Arg184, Leu188, and Pro190. A hydrogen bond exists between the hydrogen of the imidazoline ring and Pro189, at a distance of 3.08 Å, Figure 12.

Ligand **15** makes a hydrogen bond between the N-H of imidazoline and Pro189, at a distance of 2.87 Å. In addition, there are hydrophobic interactions with the amino acid residues Ile28, Ala31, Gly32, His177, Gln180, Ala181, Val183, Arg184, Leu188, and Pro190, the same interactions that were found for imidazoline **14**, Figure 13.

Finally, compound **18** does not establish hydrogen bonds, but has many hydrophobic interactions with Ala31, Gly32, His177, His179, Gln180, Ala181, Val183, Arg184, Leu188, Pro189, Ile28, and Pro190, Figures 14 and 15.

Molecular coupling assays indicate that imidazoline **13** can attach to the orthostatic site of C₆-AHL, opening the possibility of an antagonistic effect. This compound proved to decrease violacein production experimentally, which is in agreement with the findings reported by Bucio for hexyloxy phenylimidazoline [13].

Since ligands **14**, **15**, and **18** only interact with the amino acid residues of the allosteric site, they do not compete with C₆-AHL for the orthostatic site. Such an allosteric binding mode may be due to the number of carbons in the aliphatic chain of each compound.

One hypothesis is that these compounds function as positive allosteric modulators. By binding to the allosteric site, they might trigger a modification in the orthostatic site that allows for better binding by C₆-AHL. Consequently, the protein-C₆-AHL complex would form and bind to the promoter site (vioBox), thus activating and causing an enhanced transcription of the genes encoding for the enzymes involved in the synthesis of violacein.

Regarding oxazoline **16** and oxazoline **17**, the docking studies show that they bind to the orthosteric site of C₆-AHL. Although these compounds elicited a high production of violacein experimentally, they were unable to produce violacein in the absence of C₆-AHL. Hence, they are not agonists.

2.4. Molecular Dynamics, Binding Free Energy Calculations, and Per-Residue Decomposition. During docking simulations, all atoms of the receptor remained fixed. It was necessary to incorporate flexibility and solvation for all atoms of the protein-ligand complex during the docking calculations of the predicted complexes to achieve a more

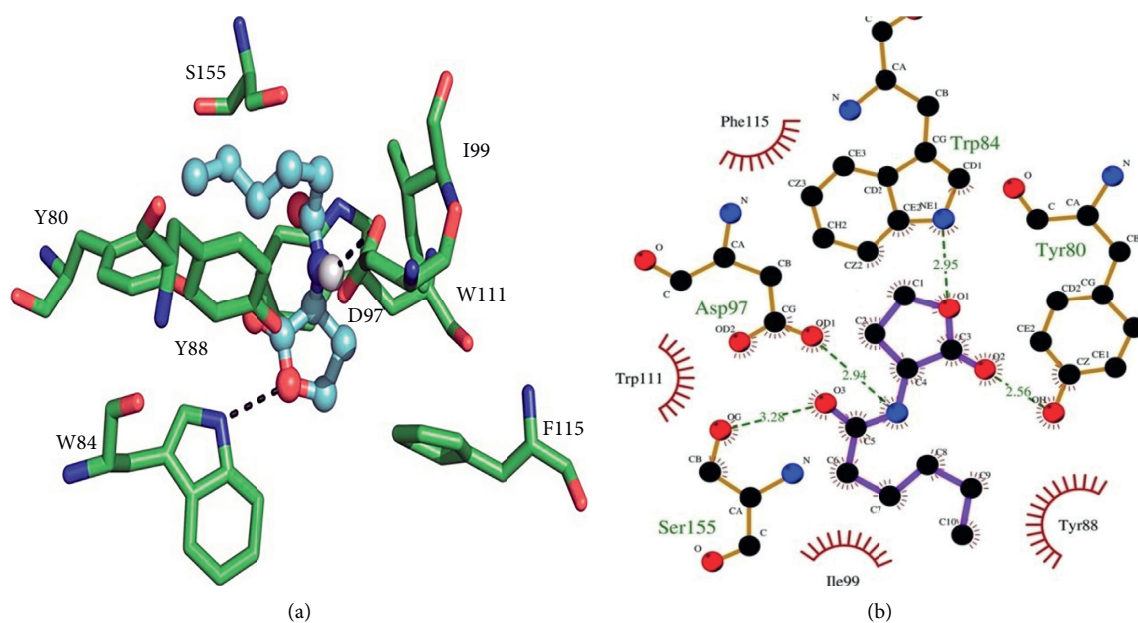


FIGURE 5: Schematic 2D diagram showing the interactions between *N*-hexanoyl homoserine lactone and CviR. The hydrophobic residues of the protein receptor that make contact with the ligand are represented by semicircles and radiant lines.

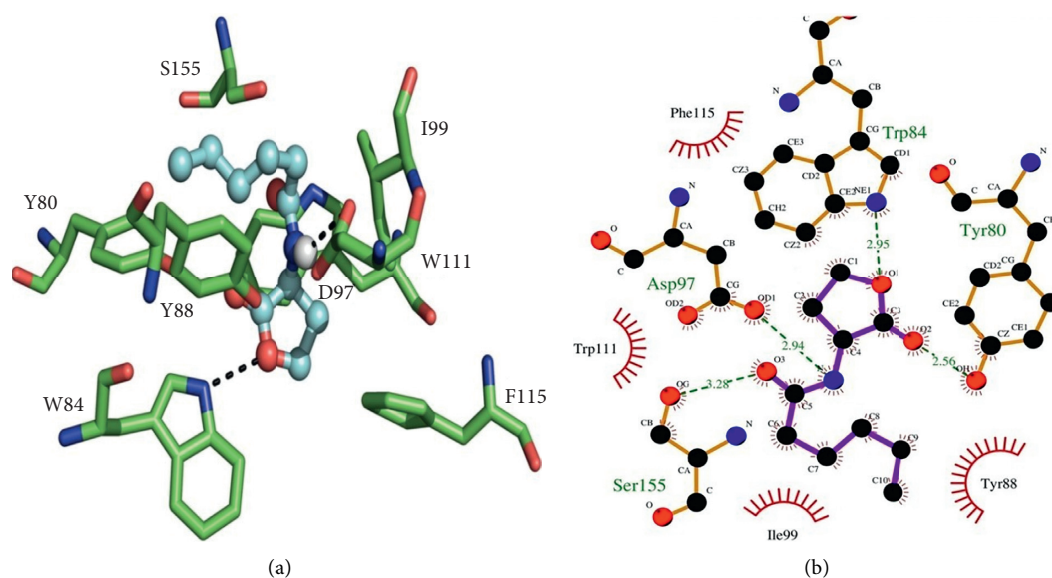


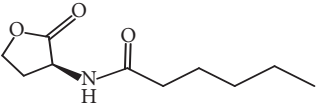
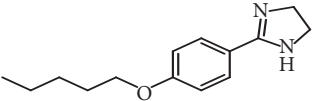
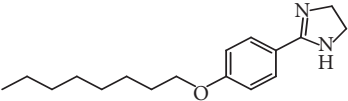
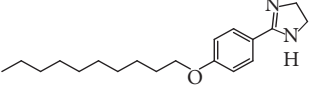
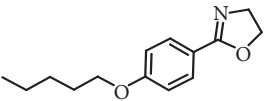
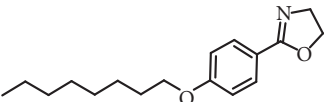
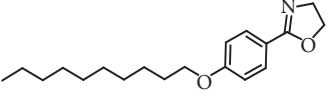
FIGURE 6: The interaction of *N*-hexanoyl homoserine lactone with CviR portrayed in 3D.

reliable result. Therefore, molecular dynamics simulations were conducted to examine the preservation of the CviR-ligand complexes for compounds **13**, **14**, and **16**.

To assess the stability of the complexes, first an RMSD analysis was made to determine the appropriate time period for a structural and energetic evaluation once reaching the equilibration stages. The CviR-**13**, CviR-**14**, and CviR-**16** systems reached equilibrated RMSD fluctuations during the first 10 ns, with average values ranging from 5.65 to 8.7 Å. Accordingly, the first 10 ns were excluded from the 50-ns-long MD simulations for the subsequent clustering analysis and binding free energy calculations.

The relative binding free energy (ΔG_{mmgbsa}), established with the MM/GBSA approach for examining CviR-ligand interactions show that all these complexes are thermodynamically favorable for binding. The main energetic contribution to ΔG_{mmgbsa} was guided by the nonpolar contributions ($\Delta E_{\text{non-polar}}$), while the polar contributions (ΔE_{polar}) were found to be unfavorable for the protein-ligand association (Table 3). The comparison of the different protein-ligand systems of the test compounds revealed that **13** and **16**, which both target the orthosteric site, bind with similar affinity. Interestingly, they exhibit a less favorable ΔG_{mmgbsa} value than **14**, even though the latter targets the allosteric site.

TABLE 2: The ΔG values for the ligand-protein interactions and the amino acid residues of the protein involved in binding.

Ligand	ΔG (kcal/mol)	Amino acid residues of the interaction site
 C ₆ -AHL, 1	-7.11	Tyr80, Trp84 [▲] , Tyr88, Asp97 [▲] , Ile99, Trp111, Phe115, Ser155
 13	-7.56	Tyr80, Trp84, Tyr88, Asp97 [▲] , Ile99, Trp111 [■] , Phe126, Met135, Ile153, Ser155 [▲]
 14	-5.95	Ile28, Ala31, Gly32, His177, GlnQ180, Val183, Arg184, Pro189 [▲]
 15	-6.02	Ile28, Ala31, Gly32, His177, Gln180, Val183, Arg184, Pro189 [▲]
 16	-7.62	Ile57, Tyr80, Trp84 [▲] , Leu85, Tyr88, Asp97, Ile99, Trp111, Phe115, Met135, Ile153, Ser155 [▲]
 17	-7.28	Ile57, Val59, Met72, Val75, Tyr80, Trp84, Leu85, Tyr88, Ile99, Met100, Trp111, Met135, Ile153, Ser155
 18	-6.14	Ala31, Gly32, His177, His179, Gln180, Ala181, Val183, Arg184, Leu188, Pro190

Hydrogen bonds (▲); π - π interactions (■).

These equations show the polar ($\Delta E_{\text{polar}} = \Delta E_{\text{ele}} + \Delta G_{\text{ele, sol}}$) and nonpolar ($\Delta E_{\text{non-polar}} = \Delta E_{\text{vwd}} + \Delta G_{\text{npol, sol}}$) contributions of ligand-protein interactions. Energy is expressed in kcal/mol (\pm standard error of the mean) and averaged over 400 snapshots at time intervals of 100 ps taken during 40 ns (after ignoring the first 10 ns of MD simulations).

To dissect the contribution of each residue to binding, analysis was made of the per-residue decomposition of each of the residues contributing to ΔG_{mmgbsa} . The key residues involved in binding and the per-residue free energy ($\Delta E_{\text{per-residue}}$) were examined for the CviR-13, Figures 16(a) and 16(b); CviR-16, Figures 16(c) and 16(d); and CviR-14, Figures 16(e) and 16(f) complexes, Figure 16. It turns out

that the CviR-13, Figures 16(a) and 16(b) and CviR-16, Figures 16(c) and 16(d), complexes are stabilized by many of the same residues. Nonetheless, the chemical differences between them leads distinct residues to provide greater contributions to the ΔG_{mmgbsa} value: Ile57, Ile99, Met100, and Trp111 for CviR-13, Figures 16(a) and 16(b); Ile57, Met72, Tyr88, and Met100 for CviR-16, Figures 16(c) and 16(d). Ile57 and Met100 are present in the stabilization of both 13 and 16, suggesting a crucial role for these residues in molecular recognition at the orthosteric site. For 14, Figures 16(e) and 16(f), on the other hand, the nonpolar protein environment implicated in stabilization is lesser for the allosteric than the orthosteric site. Pro6, Gln180, Arg184, and Pro190 contribute most to the ΔG_{mmgbsa} value.

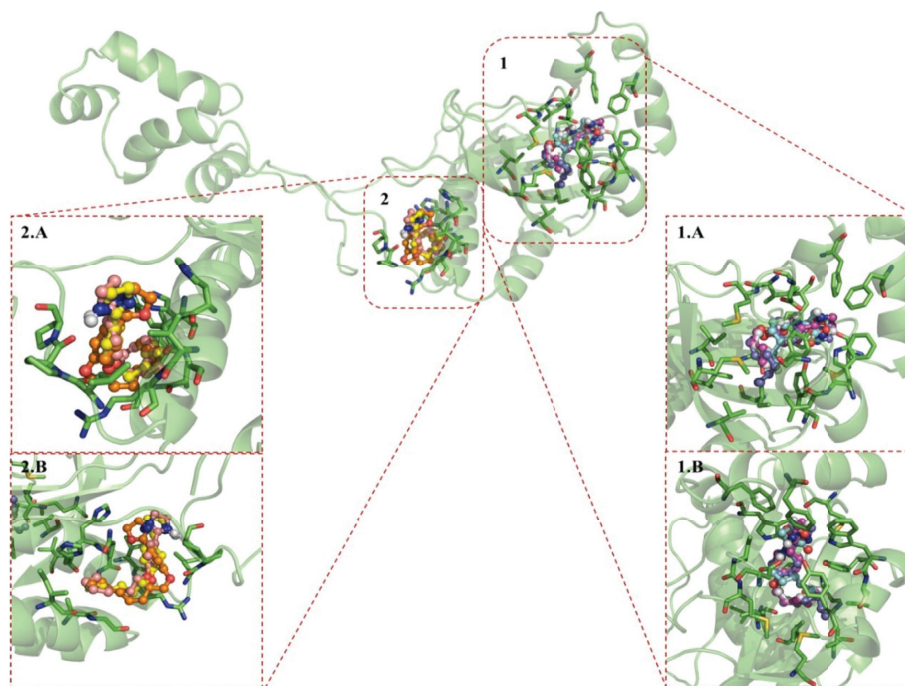


FIGURE 7: 3D illustration of the interaction of the ligands at two binding sites of the CviR protein, consisting of the orthosteric site and an allosteric site of C_6 -AHL. (1.A) Approach of the overlap of C_6 -AHL, **13**, **16**, and **17** with the amino acid residues of the active site of C_6 -AHL. (1.B) The same approach with a 45° rotation. (2.A) Approach of the overlap of **14**, **15**, and **18** with the amino acid residues of the allosteric site. (2.B) The same approach with a 45° rotation.

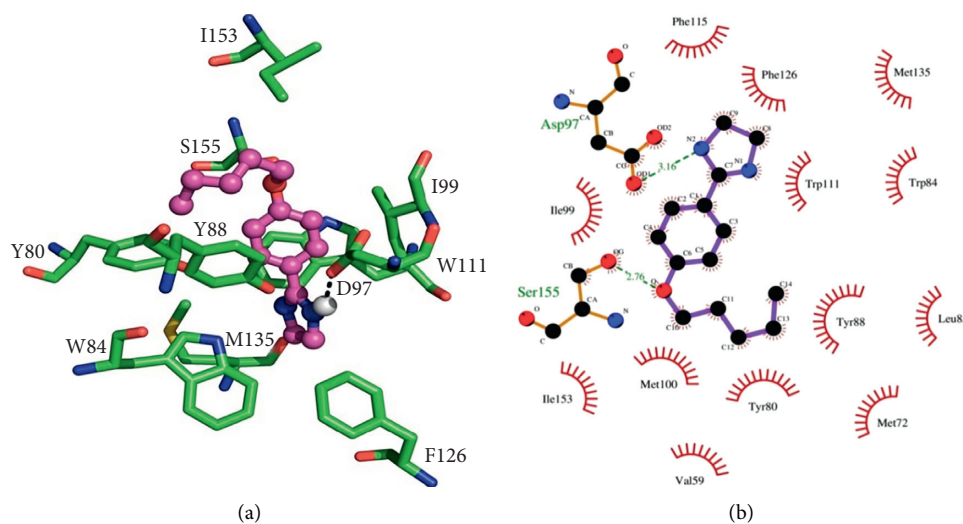


FIGURE 8: The noncovalent interaction of **13** with CviR. The ligand-protein interaction is illustrated (a) in 3D and (b) in a 2D schematic diagram. Hydrogen bonds are depicted with a dotted green line, indicating the bond distance in Å (~ 3.28). The hydrophobic residues of the protein in contact with the ligand are portrayed by red semicircles and radiant lines: Phe115.

They may be crucial residues for stabilization at the allosteric site.

3. Materials and Methods

3.1. Drying and Purification of Solvents. Ethyl acetate, methylene chloride, and hexane were purified by fractional distillation with calcium oxide (CaO) as the drying agent. The solvents were refluxed for 5 h before carrying out distillation. Ethylenediamine was also purified by fractional distillation, in

this case with metallic sodium, and refluxed under nitrogen atmosphere for 1 h. Ethylenediamine was stored at 5°C under nitrogen atmosphere and protected from light.

3.2. Characterization of the Synthesized Compounds. The organic compounds were characterized by NMR spectroscopy, mass spectrometry (MS), and infrared (IR) spectroscopy. ^1H and ^{13}C NMR spectra were recorded on a Varian Mercury spectrometer at 300 and 75 MHz and on a Varian 500 Mercury

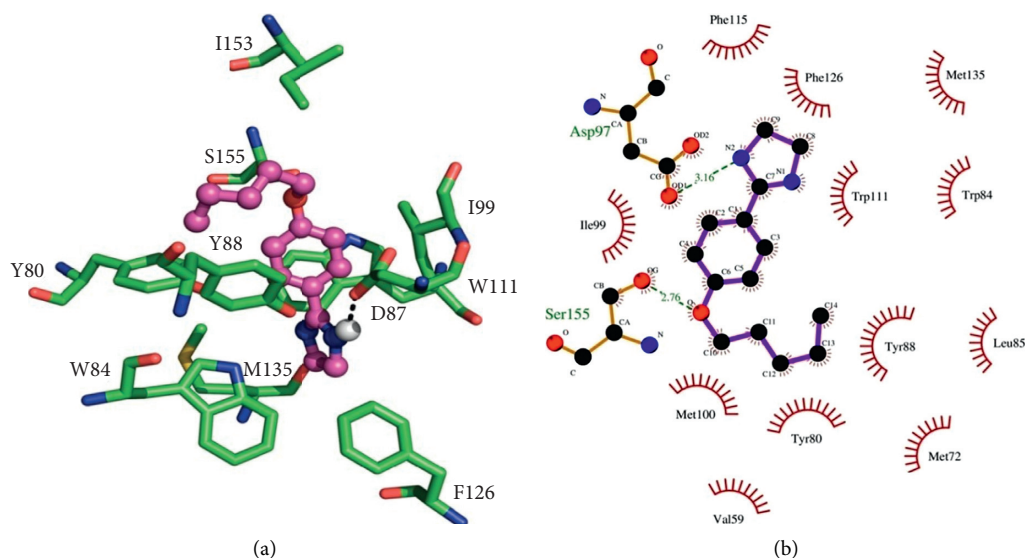


FIGURE 9: 3D portrayal of the π - π interactions between the phenyl ring of **13** and W111.

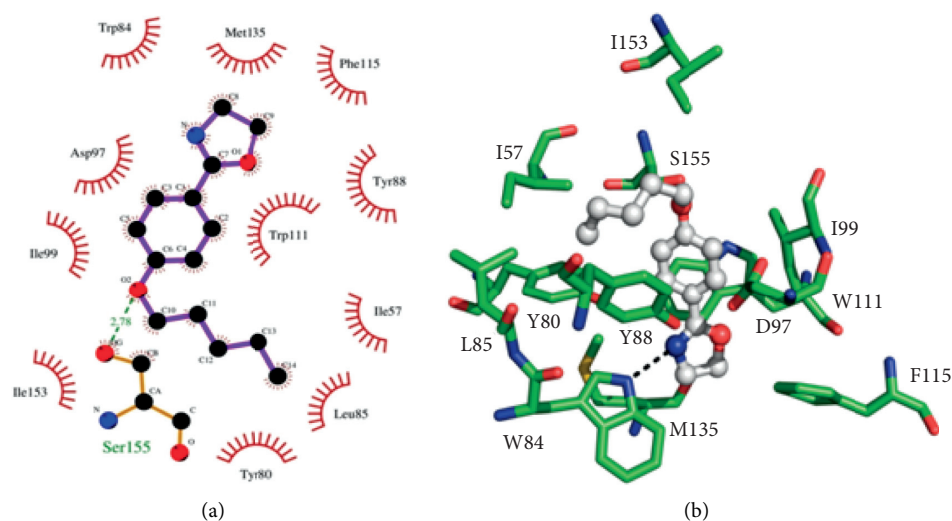


FIGURE 10: The interactions between oxazoline **16** and CviR (a) in a 2D schematic diagram and (b) in 3D.

spectrometer at 500 and 125 MHz, respectively. Infrared (IR) spectra were obtained on a Perkin Elmer FT-IR spectrum 2000 spectrometer from the ENCB-IPN spectroscopy instrumentation center. HRMS was performed with a JEOL-JSM-GC mate II and LRMS ESI(+), and spectra were recorded using a BRUKER MicroTOF QII. Melting points were determined on an electrothermal apparatus and are uncorrected.

3.3. Synthesis of Alkylated Aldehydes [13]. In a 25 mL two-neck flask, adapted with a refrigerant and magnetic stirrer and kept under nitrogen atmosphere (N_2), 4-hydroxybenzaldehyde (4.09×10^{-3} mmol) and potassium carbonate (K_2CO_3) (8.19×10^{-3} mmol, 2 eq.) were added with a funnel for solids.

Subsequently, 10 mL of distilled acetone were injected into the flask and the mixture was heated to reflux with constant stirring for 90 min. Then, the corresponding alkyl halide (5.05×10^{-3} moles, 1.5 eq.) was added and the reaction mixture was maintained at reflux with constant stirring while being monitored by TLC. After the reaction ended, the mixture was cooled to room temperature (rt), filtered, and extracted with methylene chloride (CH_2Cl_2) and the solvent was evaporated under reduced pressure in a rotary evaporator. The product was purified by silica gel column chromatography by using a polarity gradient of hexane-ethyl acetate. The fractions containing pure product were evaporated under reduced pressure and finally dried under

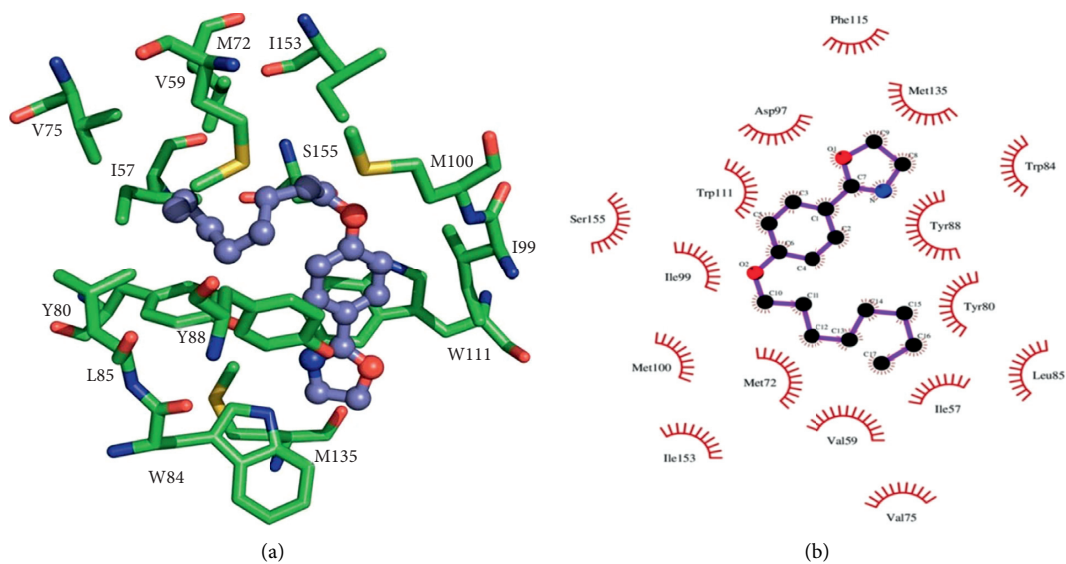


FIGURE 11: A 2D schematic diagram of the interaction between 17 and CviR.

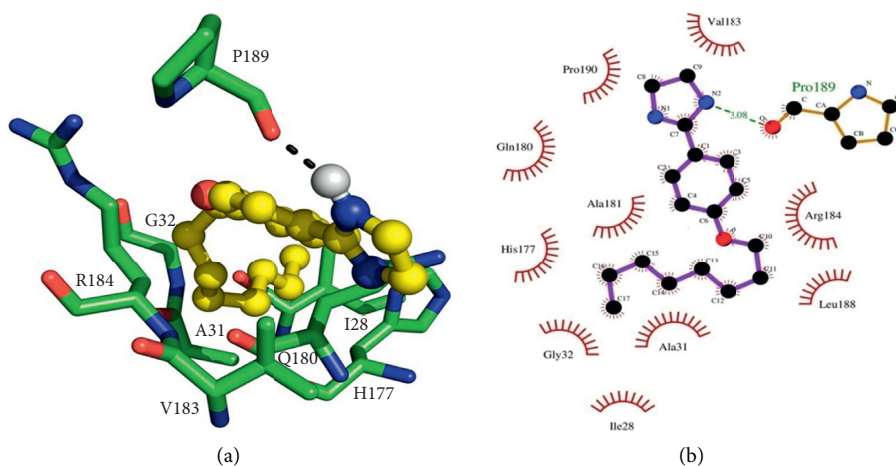


FIGURE 12: A 2D schematic diagram of the interaction between 14 and CviR.

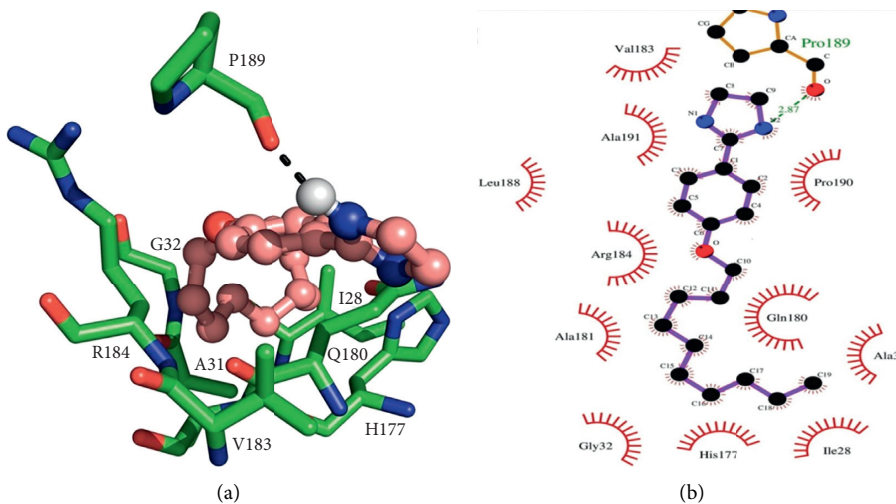
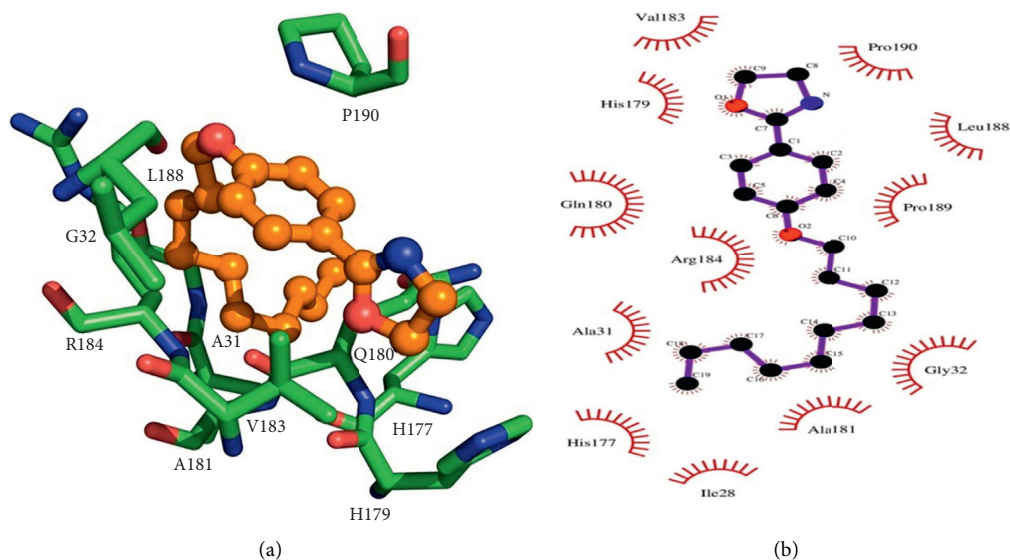
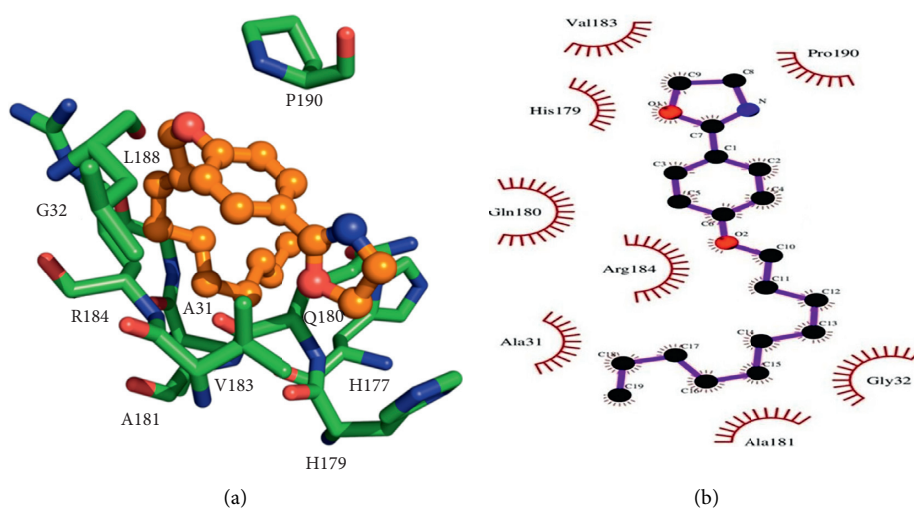
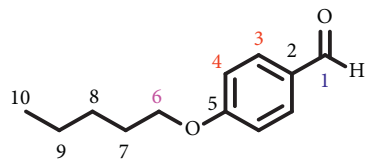


FIGURE 13: A 2D schematic diagram depicting the interactions between 15 and CviR.

FIGURE 14: A 2D schematic diagram of the interaction of **18** with CviR.FIGURE 15: The interaction of **18** with CviR shown in 3D.

a high vacuum. The resulting substances were characterized by NMR, IR, and HRMS.

3.3.1. *para*-Pentyloxy Benzaldehyde (**10**)



$\nu = 3074$ (C-H), 2931, 2870 (C-H), 1688 (C=O), 1262, 1027 (=C-O-C), and 830.

^1H NMR (CDCl_3)

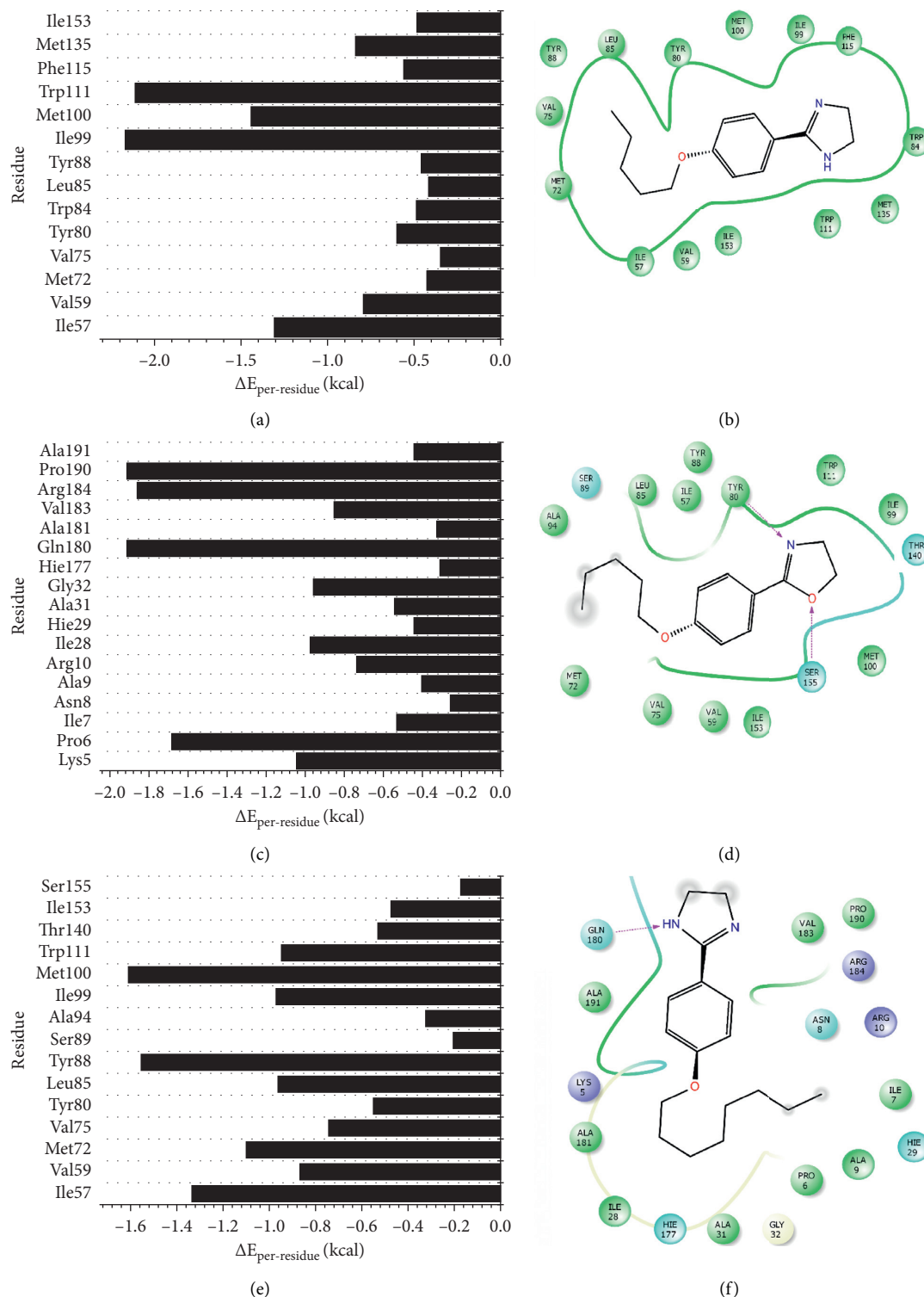
$\delta = 9.82$ (s, 1H, CHO), 7.35 (AA' BB', 4H, Ar), 3.98 (t, 2H, OCH_2), 1.76 (q, 2H, H-7), 1.38 (m, 4H, H-8y H-9), and 0.90 (t, 3H, CH_3).

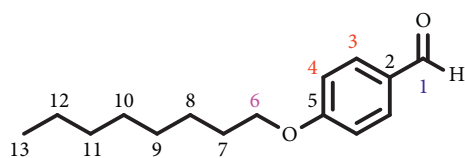
^{13}C NMR (CDCl_3)

$\delta = 190.47$ (CHO), 164.06 (C-5), 131.73 (C-3), 129.56 (C-2), 114.54 (C-4), 68.19 (C-6), 28.55 (C-7), 27.91 (C-8), 22.21 (C-9), and 13.78 (C-10).

TABLE 3: Binding free energy components of protein-ligand complexes (in units of kcal/mol).

System	ΔE_{vdw}	ΔE_{ele}	$\Delta G_{\text{ele,sol}}$	$\Delta G_{\text{npol,sol}}$	$\Delta E_{\text{non-polar}}$	ΔE_{polar}	ΔG_{mmgbsa}
13	-37.86 (0.22)	-6.07 (0.21)	21.38 (0.18)	-5.35 (0.02)	-43.21	15.31	-27.90 (0.23)
15	-45.77 (0.27)	-11.32 (0.30)	24.02 (0.26)	-5.96 (0.02)	-51.73	12.7	-39.03 (0.35)
16	-33.95 (0.30)	-14.21 (0.26)	24.69 (0.20)	-5.08 (0.03)	-39.03	10.48	-28.55 (0.27)

FIGURE 16: Per-residue free energy ($\Delta E_{\text{per-residue}}$) and map of interactions for the most populated conformation of the CviR-13 (a and b), CviR-16 (c and d), and CviR-14 (e and f) complexes. The map of interactions was constructed with Maestro Schrödinger version 10.5 [22].

3.3.2. *para*-Octyloxy Benzaldehyde (**11**)

Oil at rt

IR (KBr)

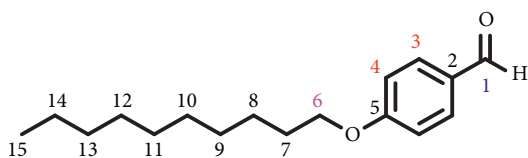
$\nu = 3074$ (C-H), 2925, 2855 (C-H), 1693 (C=O), 1255, 1019 (=C-O-C), and 830.

 ^1H NMR (CDCl_3)

$\delta = 9.71$ (s, 1H, CHO), 7.24 (AA' BB', 4H, Ar), 3.86 (t, 2H, OCH₂), 1.65 (q, 2H, H-7), 1.31 (m, 2H, H-8), 1.18 (m, 8H, H-9 al H-12), and 0.76 (t, 3H, CH₃).

 ^{13}C NMR (CDCl_3)

$\delta = 189.91$ (CHO), 163.77 (C-5), 131.39 (C-3), 129.40 (C-2), 114.27 (C-4), 67.92 (C-6), 31.39 (C-7), 28.92 (C-8), 28.82 (C-9), 28.66 (C-10), 25.56 (C-11), 22.24 (C-12), and 13.65 (C-13).

3.3.3. *para*-Decyloxy Benzaldehyde (**12**)

Oil at rt

IR (KBr)

$\nu = 3074$ (C-H), 2923, 2854 (C-H), 1696 (C=O), 1258, 1016 (=C-O-C), and 831.

 ^1H NMR (CDCl_3)

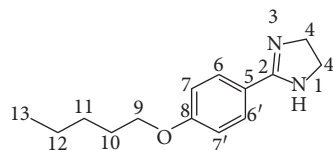
$\delta = 9.81$ (s, 1H, CHO), 7.33 (AA' BB', 4H, Ar), 3.96 (t, 2H, OCH₂), 1.75 (q, 2H, H-7), 1.41 (m, 2H, H-8), 1.27 (m, 12H, H-9 al H-14), and 0.84 (t, 3H, CH₃).

 ^{13}C NMR (CDCl_3)

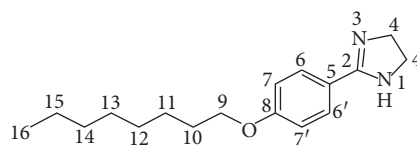
$\delta = 190.37$ (CHO), 164.06 (C-5), 131.70 (C-3), 129.58 (C-2), 114.53 (C-4), 68.20 (C-6), 31.71 (C-7), 29.38 (C-8), 29.17 (C-9), 29.14 (C-10), 28.88 (C-11), 25.78 (C-12), 22.49 (C-13), 13.95 (C-14), and 13.87 (C-15).

3.4. Synthesis of Imidazolines. In a two-neck 25 mL balloon flask adapted with a refrigerant and magnetic stirrer and kept under nitrogen atmosphere and at rt, 1 eq. of the corresponding aldehyde was added followed by the injection of 8 mL of tert-butanol and 1.1 eq. of ethylenediamine. Ninety min later, 3 eq. of K₂CO₃ and 1.25 eq. of molecular I₂ were added and the temperature was raised to 70°C. The reaction of the mixture lasted 5 h and was monitored by TLC. The system was allowed to reach rt before adding water to the reaction flask and carrying out extractions with ethyl acetate. The organic phase was washed with a saturated solution of sodium sulfite and then with a 20% NaCl

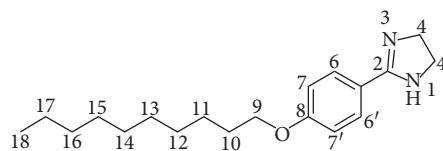
solution, and subsequently dried with anhydrous sodium sulfate. The organic phases were combined and the solvent was evaporated. The remaining residue was recrystallized from ethyl acetate.

3.4.1. 8-Pentyloxyphenyl-2-imidazoline (**13**)

m.p. 105–107°C from AcOEt. 55°C from petroleum ether; b.p. 125°/0.01 Torr [16]. IR (KBr), $\nu = 3203$ cm⁻¹ (NH) and 1618 (C=N). ^1H NMR (DMSO-D₆) $\delta = 7.34$ (AA' BB', 4H, Ph), 3.98 (t, 2H, H-9), 3.56 (s, 4H, H-4, H-4'), 1.71 (qi, 2H, H-10), 1.36 (m, 4H, H-11, H-12), and 0.89 (t, 3H, CH₃). ^{13}C NMR (DMSO-D₆) $\delta = 163.03$ (C-2), 160.00 (C-8), 128.45 (C-6), 122.78 (C-5), 113.70 (C-7), 67.34 (C-9), 49.17 (C-4, C-4'), 28.14 (C-10), 27.51 (C-11), 21.17 (C-12), and 13.71 (C-13). HRMS, m/z = calculated for C₁₄H₂₁N₂O (M⁺): 233.1648; found 233.1625.

3.4.2. 8-Octyloxyphenyl-2-imidazoline (**14**)

m.p. 115–117°C from AcOEt. m.p. 109°C from benzene: hexane [17]. IR (KBr) $\nu = 3209$ cm⁻¹ (NH) and 1618 (C=N). ^1H NMR (DMSO-D₆) $\delta = 6.95$ (AA' BB', 4H, Ph), 3.99 (t, 2H, H-9), 3.60 (s, 4H, H-4, H-4'), 1.72 (qi, 2H, H-10), 1.39 (m, 2H, H-11), 1.27 (m, 8H, H-12, H-13, H-14, H-15), and 0.86 (t, 3H, CH₃). ^{13}C NMR (DMSO-D₆) $\delta = 163.28$ (C-2), 160.43 (C-8), 128.77 (C-6), 122.23 (C-5), 113.96 (C-7), 67.57 (C-9), 49.10 (C-4, C-4'), 31.12 (C-10), 28.72 (C-11), 28.65 (C-12), 28.60 (C-13), 25.48 (C-14), 22.07 (C-15), and 13.93 (C-16). HRMS, m/z = calculated for C₁₇H₂₆N₂O (M⁺): 275.2118; found 275.2099.

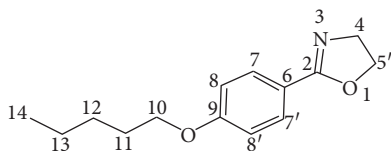
3.4.3. 8-Decyloxyphenyl-2-imidazoline (**15**)

m.p. 151–153°C IR (KBr), $\nu = 3132$ cm⁻¹ (NH) and 1614 (C=N). ^1H NMR (DMSO-D₆) $\delta = 7.56$ (AA' BB', 4H, Ph), 4.09 (t, 2H, H-9), 3.98 (s, 4H, H-4, H-4'), 1.73 (qi, 2H, H-10), 1.41 (m, 2H, H-11), 1.29 (m, 12H, H-12, H-13, H-14, H-15, H-16, H-17), and 0.84 (t, 3H, CH₃). ^{13}C

NMR (DMSO- D_6) δ = 164.43 (C-2), 163.67 (C-8), 130.79 (C-6), 115.32 (C-7), 113.93 (C-5), 68.38 (C-9), 44.35 (C-4, C-4'), 31.42 (C-10), 29.12 (C-11), 29.07.18 (C-12), 28.84 (C-13), 28.82 (C-14), 28.56 (C-15), 25.53 (C-16), 22.23 (C-17), and 14.08 (C-18). HRMS, m/z = calculated for $C_{19}H_{30}N_2O$ (M^+): 303.2431; found 303.2467.

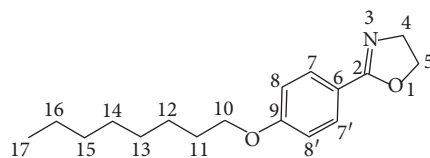
3.5. Synthesis of Oxazolines. To a 200 mL MW reactor flask, adapted with a refrigerant and a magnetic stirrer, 1 eq. of the corresponding aldehyde (depending on the oxazoline to be synthesized) followed by the injection of 5 mL of t-BuOH and 1.1 eq. of ethanolamine were added. The flask was placed in a chemical microwave oven (model MIC-1, Prendo), and the conditions for the reaction were programmed (50°C, 3 min 14 s, 1290 rpm, and 60% power at 762 watts). After this cycle, 3 eq. of K_2CO_3 and then of 1.5 eq. of I_2 were added and the reaction conditions were changed (78°C, 20 min 14 s, 1290 rpm, and 60% power at 762 Watts). The reaction, monitored by TLC, ended upon completion of 5 cycles. Once the system reached rt, the organic phase was separated and water was added to the reaction flask. Potassium carbonate was solubilized (aqueous phase), and extractions were carried out by using ethyl acetate. The organic phase was washed with a saturated solution of sodium sulfite (Na_2SO_3) and then with a 20% NaCl solution, and subsequently dried with anhydrous sodium sulfate. The ethyl acetate was evaporated under reduced pressure. The mixture of the product and remaining raw material were separated by silica gel column chromatography by using a polarity gradient of hexane-ethyl acetate. The solvent was evaporated from the pure fractions and the purified product dried under a high vacuum.

3.5.1. 9-Pentyloxy phenyl-2-oxazoline (16)



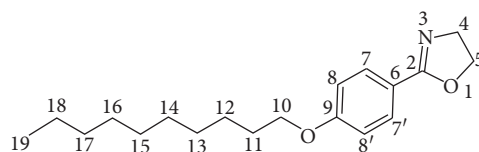
m.p. 36–38°C. IR (KBr), ν = 1649 cm^{-1} (C=N). 1H NMR (DMSO- D_6) δ = 6.96 (AA' BB', 4H, Ph), 4.35 (t, 2H, H-5), 3.99 (t, 2H, H-10), 3.90 (t, 2H, H-4), 1.71 (m, 2H, H-11), 1.35 (m, 2H, H-12, H-13), and 0.88 (t, 3H, CH_3). ^{13}C NMR (DMSO- D_6) δ = 162.70 (C-2), 161.06 (C-9), 129.46 (C-7), 119.81 (C-6), 114.35 (C-8), 67.68 (C-10), 67.18 (C-5), 54.37 (C-4), 28.31 (C-11), 27.67 (C-12), 21.91 (C-13), and 13.97 (C-14). HRMS, m/z = calculated for $C_{14}H_{29}NO_2$ (M^+): 234.1489; found 234.1529.

3.5.2. 9-Octyloxy phenyl-2-oxazoline (17)



m.p. 41–43°C. IR (KBr), ν = 1644 cm^{-1} (C=N). 1H NMR ($CDCl_3$) δ = 6.88 (AA' BB', 4H, Ph), 4.39 (t, 2H, H-5), 4.03 (t, 2H, H-10), 3.98 (t, 2H, H-4), 1.78 (m, 2H, H-11), 1.45 (m, 2H, H-12), 1.32 (m, 8H, H-13, H-14, H-15, H-16), and 0.88 (t, 3H, CH_3). ^{13}C NMR ($CDCl_3$) δ = 165.16 (C-2), 161.69 (C-9), 127.01 (C-7), 117.05 (C-6), 111.37 (C-8), 65.33 (C-10), 64.68 (C-5), 52.08 (C-4), 29.04 (C-11), 26.55 (C-12), 26.43 (C-13), 26.38 (C-14), 23.23 (C-15), 19.88 (C-16), and 11.31 (C-17). HRMS, m/z = calculated for $C_{17}H_{25}NO_2$ (M^+): 276.1958; found 276.2000.

3.5.3. 9-Decyloxy phenyl-2-oxazoline (18)



m.p. 48–50°C. IR (KBr), ν = 1650 cm^{-1} (C=N). 1H NMR (DMSO- D_6) δ = 6.97 (AA' BB', 4H, Ph), 4.35 (t, 2H, H-5), 4.00 (t, 2H, H-10), 3.91 (t, 4H, H-4, H-4'), 1.71 (m, 2H, H-11), 1.40 (m, 2H, H-12), 1.28 (m, 12H, H-13, H-14, H-15, H-16, H-17, H-18), and 0.85 (t, 3H, CH_3). ^{13}C NMR (DMSO- D_6) δ = 162.65 (C-2), 161.00 (C-9), 129.41 (C-7), 119.75 (C-6), 114.31 (C-8), 67.63 (C-10), 67.13 (C-5), 54.31 (C-4), 31.28 (C-11), 28.98 (C-12), 28.93 (C-13), 28.73 (C-14), 28.68 (C-15), 28.55 (C-16), 25.44 (C-17), 22.08 (C-18), and 13.92 (C-19). HRMS, m/z = calculated for $C_{19}H_{29}NO_2$ (M^+): 304.246; found 304.2316.

3.6. Preparation of Culture Media, Test Compounds, and Inoculum. The Luria Bertani (LB) broth was prepared in one liter of distilled water by adding 10 g peptone, 5 g yeast extract, and 5 g NaCl and then sterilized in an autoclave at 15 psi and 121°C for 15 min. For the LB solid medium, 15 g of bacteriological agar was added to a liter of distilled water. *C. violaceum* CV026 was always grown in the presence of 30 μg /mL of kanamycin.

The amount of each compound required for a concentration of 100 mM was weighed. With the resulting solution, serial dilutions 1:10 were made to obtain the concentrations of 1000 μM , 100 μM , 10 μM , 1 μM , and 0.1 μM .

From the cryovials containing *C. violaceum* CV026, a roast was taken and crosswise streaked in a box containing LB agar and 30 $\mu\text{g}/\text{mL}$ kanamycin, followed by incubation at 29°C for 24 h. A roast was also taken from an isolated colony and inoculated in 5 mL LB medium with 30 $\mu\text{g}/\text{mL}$ kanamycin for CV026, followed by incubation at 29°C and 200 rpm for 15 h. Finally, the boxes were stored in a refrigerator.

3.7. Evaluation of the Compounds as Quorum-Sensing Inhibitors in *Chromobacterium violaceum* CV026. *C. violaceum* CV026 was cultured in 60 mL of the LB medium with 30 $\mu\text{g}/\text{mL}$ kanamycin until reaching an optical density of 0.1 to 600 nm. Subsequently, in 2 mL tubes, 980 μL of this culture, 80 μM C_6 -AHL (800 nM final concentration), and 10 μL of the dilutions of the test compounds were added until reaching the final concentration of 1000 μM , 100 μM , 10 μM , 1 μM , and 0.1 μM . Then, the tubes were incubated at 29°C and 700 rpm for 24 h. Upon completion of the incubation time, cell density was determined by absorbance at 720 nm by using the LB medium as the blank. Finally, the absorbance of violacein was measured.

3.8. Evaluation of Violacein. 500 μL of the bacterial culture was placed in a 2 mL tube and 500 μL of acetone were added. The tubes were vortexed and centrifuged at 15000 rpm for 4 min to prepare for the determination of the absorbance of violacein in the supernatants at 577 nm. The specific production of violacein was calculated by dividing the value of the reading at 577 nm by that at 720 nm. Each experiment was performed 6 times/compound, and the results were graphed. Statistical significance was analyzed by ANOVA.

3.9. Viable Count. From the 24 h cultures of the test compounds, 10 μL were taken to make decimal dilutions and 5 μL of each dilution was dripped onto plates containing the LB agar. After incubation at 29°C for 24 h, the colonies on each spot were counted. These assays were performed in triplicate, and viable counts were confirmed by standard bacterial plating.

3.10. Assay of the Compounds as Agonists. A flask containing 60 mL of the LB medium with kanamycin was adjusted to an optical density of 0.1 to 600 nm with *C. violaceum* CV026. Subsequently, 990 μL of this solution were placed in 2 mL tubes and 10 μL of the dilutions of the compounds were added until reaching a final concentration of 1000 μM , 100 μM , 10 μM , 1 μM , and 0.1 μM . Moreover, a positive control (990 μL culture + 10 μL of an 80 μM solution of C_6 -AHL) and a negative control (990 μL culture + 10 μL of the LB medium) were included. The tubes were incubated at 29°C while subjected to shaking at 700 rpm for 24 h. The presence or absence of pigment was then observed to make an evaluation of violacein.

3.11. Determination of MIC in *Chromobacterium violaceum* CV026. The procedure described in section 3.7 was followed, except that the final concentration of the compounds was from 10 to 1000 μM . The MIC was assigned to the lowest concentration of the compound yielding no bacterial development.

3.12. Modeling and Optimization of Ligands. Docking studies were carried out on the ligands tested experimentally in *C. violaceum* CB026 and on the natural ligand of the CviR protein. The ligands were built with the ACD/ChemSketch program, creating a geometric preoptimization in 3D (respecting the stereochemistry and spatial configuration). The structures were saved in .mol format, and these files served as an input to create the **Z** matrix for each molecule on the GaussView 5.0 graphical visualizer. The files were saved in .gjp input format for their use in Gaussian 09. The structures obtained (and their respective matrices **Z**) were submitted to a geometric and energetic optimization at the AM1 semiempirical level with the chemical-quantum package of Gaussian 09. The output files in .out format were transformed into 3D format.pdb with the GaussView 5.0 program. The latter files were utilized for simulations by molecular coupling.

3.13. Molecular Studies. With docking studies, an initial examination was made of each ligand-binding site on the CviR protein as well as the ligand-receptor interactions. *C. violaceum* 12472 (located in the Protein Data Bank under the PDB code: 3QP6) was chosen as the target protein for this analysis on the AutoDock 4.2 program, which maintains the macromolecule rigid while allowing flexibility in the ligand [23]. The AutoDock 4.2 program has shown good correlation between the free energy values of the binding simulations and the experimental data [24]. Blind docking was carried out with a grid box of $126 \times 126 \times 126 \text{ \AA}^3$ and a 0.375 \AA^3 space between grid points and by using the Hybrid Genetic Algorithm of Lamarckian with an initial population of 100 randomized individuals and a maximum number of energy evaluations of 1×10^7 . The results of the simulations were examined by means of the PyMol visualizer, observing the amino acid residues of the protein involved in the interactions with the ligands. 2D protein-ligand interaction diagrams were generated with the LIGPLOT program, revealing additional amino acid residues that interact with the ligands.

3.14. Molecular Dynamics Simulations and Binding Free Energy Calculations. MD simulations of the CviR-ligand systems were conducted with the PMEMD module AMBER12 package [25], the ff99SB force field [26], and the generalized Amber force field (GAFF) [27]. A 12 \AA rectangular-shaped box of TIP3P water molecules [28] was constructed to solvate the CviR-ligand complexes, and counterions were placed at different locations to neutralize the charges of the complexes at pH 7. Systems were minimized and equilibrated by carrying out a protocol that began

with 1000 steps of steepest descent minimization and continued with 1000 steps of conjugate gradient minimization. Equilibrations began by heating the systems from 0 to 310 K during 200 picoseconds (ps) of MD simulations, with position restraints set at a constant volume. Successive MD simulations were conducted under periodic boundary conditions (PBCs) using an isothermal isobaric (NpT) ensemble of 200 ps to adjust the solvent density, followed by 800 ps of constant pressure equilibration at 310 K (with the SHAKE algorithm) [29] on hydrogen atoms using a time step of 2 femtoseconds (fs) and Langevin dynamics for temperature control. Subsequent to equilibrations, 50-ns-long MD simulations were conducted in the absence of position restraints, under PBCs and with an NpT ensemble at 310 K. A 10 Å cutoff was applied for the van der Waals interactions. The electrostatic term was described via the particle mesh Ewald method [30], and bond lengths were constrained at their equilibrium values with the SHAKE algorithm [29]. Temperature and pressure were maintained by utilizing the weak-coupling algorithm [31] with coupling constants τ_T and τ_P of 1.0 and 0.2 ps, respectively (310 K, 1 atm). The time dependence of the MD simulation runs was analyzed by employing AmberTools from Amber12. On the other hand, structural representations were created with PyMOL v0.99 [32] and Maestro Schrödinger version 10.5 [22].

3.15. Calculation of Relative Binding Free Energies and Per-Residue Contributions. Relative binding free energies were calculated according to the MMGBSA [33–36] provided in Amber12 [25]. For this purpose, 400 snapshots at time intervals of 100 ps were extracted during 40 ns, ignoring the first 10 ns of the 50-ns-long MD simulations, using a salt concentration of 0.1 M and the Born implicit solvent model [36] after removing water molecules and counterions. The analyses were performed with the MMPBSA Perl script [35]. The binding free energy of each complex can be calculated as follows:

$$\Delta G_{\text{mmgbsa}} = G^{\text{complex}} - G^{\text{receptor}} - G^{\text{ligand}}, \quad (1)$$

$$\Delta G_{\text{bind}} = \Delta E_{\text{MM}} + \Delta G_{\text{solvation}} - T\Delta S.$$

4. Conclusions

Six azolines were synthesized, including three imidazolines obtained in moderate yields by conventional heating and three oxazolines afforded in good yields by MW. The performance of the azolines was dependent on the size of the chains of the alkoxy benzaldehydes. A significant increase in violacein production was induced (in the presence of hexanoyl homoserine lactone) by 8-decyloxyphenyl-2-imidazole **17** (**15**) (10 μM), 9-decyloxyphenyl-2-oxazoline **20** (**18**) (10, 100, and 1000 μM), 9-pentyloxyphenyl-2-oxazoline **18** (**16**) (10 and 100 μM), and 9-octyloxyphenyl-2-oxazoline **19** (**17**) (100 and 1000 μM). An inhibitory effect on violacein production was shown by 8-pentyloxyphenyl-2-imidazole **15** (**13**), with an IC_{50} of 56.38 μM , strongly suggesting an

antiquorum sensing effect. This was the most active compound in the homologous series. Of the imidazolines currently under study, those with anti-QS activity had an aliphatic chain similar in size to that of C_6 -AHL. An inhibitory effect on the growth of *C. violaceum* CV026 was elicited by 100 and 1000 μM of imidazole **17** (**15**), 100 μM of imidazole **16** (**14**), and 1000 μM of oxazoline **18** (**16**). Quorum-sensing agonist activity was not found for any of the test compounds. The experimental inhibitory effect on violacein production promoted by **15** (**13**) was in agreement with the docking study. Ten amino acid residues in the active site of the receptor protein were involved in the interactions with 8-pentyloxyphenyl-2-imidazole. Seven of these 10 also interacted with AHL. Additionally, one of them is implicated in π - π interactions.

Data Availability

The data used to support the findings of this study are available from the corresponding author upon request.

Conflicts of Interest

The authors declare that there are no conflicts of interest regarding the publication of this paper.

Authors' Contributions

A.R.-A. was involved in conceptualization; A.R.-A., E.C.-Q., and J.C.-B. were involved in methodology; J.C.-B., M.B., and J.L.H.-A were responsible for software; A.R.-A., E.C.-Q., and J.C.-B. validated the study; A.R.-A., E.C.-Q., J.C.-B., J.L.H.-A., and M.B. performed formal analysis; J.L.H.-A. and M.B. performed investigation; A.R.-A., E.C.-Q., and J.C.-B. were responsible for resources; A.R.-A. curated the data; A.R.-A., E.C.-Q., and J.C.-B. wrote and prepared the original draft; A.R.-A. wrote, reviewed, and edited the manuscript; A.R.-A. was involved in visualization; A.R.-A. supervised the study; A.R.-A. was involved in project administration; A.R.-A was involved in funding acquisition.

Acknowledgments

AR is grateful to IPN for the financial support through grant SIP20181666 and to CONACyT for grants 240808 and 255420. JC is grateful to CONACyT for the financial support through grant 254600. JLHA is appreciative of scholarships provided by CONACyT and the IPN. The authors are beholden to CNMN, IPN, for HRMS and to CE, ENCB, for IR spectra.

Supplementary Materials

Selected ^1H NMR-, ^{13}C NMR-, HSQC- HMBC- IR-, and HRMS-spectra. (*Supplementary Materials*)

References

- [1] G. M. Dunny and B. A. B. Leonard, "Cell-cell communication in Gram-positive bacteria," *Annual Review of Microbiology*, vol. 51, no. 1, pp. 527–564, 1997.

- [2] M. B. Miller and B. L. Bassler, "Quorum sensing in bacteria," *Annual Review of Microbiology*, vol. 55, no. 1, pp. 165–199, 2001.
- [3] A. Jayaraman and T. K. Wood, "Bacterial quorum sensing: signals, circuits, and implications for biofilms and disease," *Annual Review of Biomedical Engineering*, vol. 10, no. 1, pp. 145–167, 2008.
- [4] C. Fuqua and E. P. Greenberg, "Listening in on bacteria: acyl-homoserine lactone signalling," *Nature Reviews Molecular Cell Biology*, vol. 3, no. 9, pp. 685–695, 2002.
- [5] J. P. Gerdt and H. E. Blackwell, "Competition studies confirm two major barriers that can preclude the spread of resistance to quorum-sensing inhibitors in bacteria," *ACS Chemical Biology*, vol. 9, no. 10, pp. 2291–2299, 2014.
- [6] K. Chong-Lek, S. Choon-Kook, Y. Wai-Fong et al., "Plant-derived natural products as sources of anti-quorum sensing compounds," *Sensors*, vol. 13, no. 5, pp. 6217–6228, 2013.
- [7] M. D. L. Fuente, C. D. Miranda, P. Jopia et al., "Growth inhibition of bacterial fish pathogens and quorum-sensing blocking by bacteria recovered from Chilean salmonid farms," *Journal of Aquatic Animal Health*, vol. 27, no. 2, pp. 112–122, 2015.
- [8] M. Manefield, R. De Nys, K. Naresh et al., "Evidence that halogenated furanones from *Delisea pulchra* inhibit acylated homoserine lactone (AHL)-mediated gene expression by displacing the AHL signal from its receptor protein," *Microbiology*, vol. 145, no. 2, pp. 283–291, 1999.
- [9] S. Majumdar and S. Mondal, "Perspectives on quorum sensing in fungi," *IJMBM*, vol. 6, pp. 170–180, 2015.
- [10] M. A. Welsh, N. R. Eibergen, J. D. Moore, and H. E. Blackwell, "Small molecule disruption of quorum sensing cross-regulation in *Pseudomonas aeruginosa* causes major and unexpected alterations to virulence phenotypes," *Journal of the American Chemical Society*, vol. 137, no. 4, pp. 1510–1519, 2015.
- [11] J. E. Galván, M. E. Defonsi Lestard, O. E. Piro et al., "Synthesis, characterization and crystal structure of 2-chloroethyl(methylsulfonyl)methanesulfonate," *New Journal of Chemistry*, vol. 42, no. 13, pp. 11073–11084, 2018.
- [12] A. Reyes-Arellano, A. Bucio-Cano, M. Montenegro-Sustaita, E. Curiel-Quesada, and H. Salgado-Zamora, "Imidazolines as non-classical bioisosteres of *N*-acyl homoserine lactones and quorum sensing inhibitors," *International Journal of Molecular Sciences*, vol. 13, no. 2, pp. 1284–1299, 2012.
- [13] V. B. Maisuria and A. S. Nerurkar, "Interference of quorum sensing by *delftia* sp. VM4 depends on the activity of a novel *N*-acylhomoserine lactone-acylase," *PLoS One*, vol. 10, no. 9, Article ID e0138034, 2015.
- [14] A. Bucio-Cano, A. Reyes-Arellano, J. Correa-Basurto et al., "Targeting quorum sensing by designing azoline derivatives to inhibit the *N*-hexanoyl homoserine lactone-receptor CviR: synthesis as well as biological and theoretical evaluations," *Bioorganic & Medicinal Chemistry*, vol. 23, no. 24, pp. 7565–7577, 2015.
- [15] V. Kothari, S. Sharma, and D. Padia, "Recent research advances on *Chromobacterium violaceum*," *Asian Pacific Journal of Tropical Medicine*, vol. 10, no. 8, pp. 744–752, 2017.
- [16] W. Koller and P. Schlack, "Ein neues Darstellungsverfahren für 2-Aryl- Δ 1-pyrroline und 2-Aryl- Δ 1-piperideine," *Chemische Berichte*, vol. 96, pp. 93–113, 1963.
- [17] H. Morton, F. E. Soroko, and G. M. McKenzie, "2-(Alkoxyaryl)-2-imidazoline monoamine oxidase inhibitors with antidepressant activity," *Journal of Medicinal Chemistry*, vol. 21, no. 1, pp. 405–409, 1978.
- [18] K. Goossens, S. Wellens, K. Van Hecke, L. Van Meervelt, T. Cardinaels, and K. Binnemans, "T-shaped ionic liquid crystals based on the imidazolium motif: exploring substitution of the C-2 imidazolium carbon atom," *Chemistry-A European Journal*, vol. 17, no. 15, pp. 4291–4306, 2011.
- [19] G. Chen, L. R. Swem, D. L. Swem et al., "A strategy for antagonizing quorum sensing," *Molecular Cell*, vol. 42, no. 2, pp. 199–209, 2011.
- [20] D. Martinelli, G. Grossmann, U. Séquin, H. Brandl, and R. Bachofen, "Effects of natural and chemically synthesized furanones on Quorum Sensing in *Chromobacterium violaceum*," *BMC Microbiology*, vol. 4, no. 1, p. 25, 2004.
- [21] G. M. Morris, R. Huey, W. Lindstrom et al., "AutoDock4 and AutoDockTools4: automated docking with selective receptor flexibility," *Journal of Computational Chemistry*, vol. 30, no. 16, pp. 2785–2791, 2009.
- [22] Maestrovol. 5 Schrödinger, LLC, New York, NY, USA, 2016.
- [23] G. M. Morris, S. D. Goodsell, S. Halliday et al., "Automated docking using a Lamarckian genetic algorithm and an empirical binding free energy function," *Journal of Computational Chemistry*, vol. 19, no. 14, pp. 1639–1662, 1998.
- [24] A. Patronov, I. Dimitrov, D. R. Flower, and I. Doytchinova, "Peptide binding prediction for the human class II MHC allele HLA-DP2: a molecular docking approach," *BMC Structural Biology*, vol. 11, no. 1, p. 32, 2011.
- [25] D. A. Case, T. E. Cheatham, T. Darden et al., "The Amber biomolecular simulation programs," *Journal of Computational Chemistry*, vol. 26, no. 16, pp. 1668–1688, 2005.
- [26] Y. Duan, C. Wu, S. Chowdhury et al., "A point-charge force field for molecular mechanics simulations of proteins based on condensed-phase quantum mechanical calculations," *Journal of Computational Chemistry*, vol. 24, no. 16, pp. 1999–2012, 2003.
- [27] J. Wang, R. M. Wolf, J. W. Caldwell, P. A. Kollman, and D. A. Case, "Development and testing of a general amber force field," *Journal of Computational Chemistry*, vol. 25, no. 9, pp. 1157–1174, 2004.
- [28] W. L. Jorgensen, J. Chandrasekhar, J. D. Madura, R. W. Impney, and M. L. Klein, "Comparison of simple potential functions for simulating liquid water," *The Journal of Chemical Physics*, vol. 79, no. 2, pp. 926–935, 1983.
- [29] W. F. van Gunsteren and H. J. C. Berendsen, "Algorithms for macromolecular dynamics and constraint dynamics," *Molecular Physics*, vol. 34, no. 5, pp. 1311–1327, 1977.
- [30] T. Darden, D. York, and L. Pedersen, "Particle mesh Ewald: an N -log(N) method for Ewald sums in large systems," *The Journal of Chemical Physics*, vol. 98, no. 12, pp. 10089–10092, 1993.
- [31] H. J. C. Berendsen, J. P. M. Postma, W. F. van Gunsteren, A. DiNola, and J. R. Haak, "Molecular dynamics with coupling to an external bath," *The Journal of Chemical Physics*, vol. 81, no. 8, pp. 3684–3690, 1984.
- [32] W. L. DeLano, *The PyMOL Molecular Graphics System*, DeLano Scientific, Palo Alto, CA, USA, 2002, <http://www.pymol.org>.
- [33] B. R. Miller, T. D. McGee, J. M. Swails, N. Homeyer, H. Gohlke, and A. E. Roitberg, "MMPBSA.PY: an efficient program for end-state free energy calculations," *Journal of Chemical Theory and Computation*, vol. 8, no. 9, pp. 3314–3321, 2012.
- [34] P. A. Kollman, I. Massova, C. Reyes et al., "Calculating structures and free energies of complex molecules: combining molecular mechanics and continuum models," *Accounts of Chemical Research*, vol. 12, p. 897, 2000.

- [35] J. Gohlke, W. Griffith, and E. M. Faustman, "The role of cell death during neocortical neurogenesis and synaptogenesis: implications from a computational model for the rat and mouse," *Developmental Brain Research*, vol. 151, p. 54, 2004.
- [36] A. Onufriev, D. Bashford, and D. A. Case, "Exploring protein native states and large-scale conformational changes with a modified generalized born model," *Proteins: Structure, Function, and Bioinformatics*, vol. 55, no. 2, pp. 383–394, 2004.